Strengthened MIP Formulations for the Liver Region Redesign Models of Akshat et al.

Aysenur Karagoz[a], Ruofeng Liu[a], Hamidreza Validi[1b], Andrew J. Schaefer[a]

[a]*Department of Computational Applied Mathematics & Operations Research, Rice University, TX, US*
[b]*Department of Industrial, Manufacturing & Systems Engineering, Texas Tech University, TX, US*

Abstract

Liver transplantation has been a critical issue in the U.S. healthcare system for decades, and the region redesign aims to ameliorate this issue. This paper revisits two mixed integer programming (MIP) formulations of the liver region redesign problem proposed by Akshat et al. [2]. We study their first formulation considering two different modeling approaches: one compact formulation and one with exponentially many constraints. We also propose a set of variable fixing procedures and conduct a polyhedral study on their second formulation. Our computational results show that multiple unsolved instances are solved to optimality.

Keywords: liver transplant allocation, mixed integer programming, polyhedral theory

1. Introduction

Chronic liver disease/cirrhosis is one of the leading causes of death in the US, and transplantation is the only treatment. In 2022, there were over 50,000 deaths attributed to liver disease in the U.S. The demand for liver transplants is rising due to various factors, including the increasing prevalence of liver diseases, as well as an aging population. As of 2023, more than 10,000 people are on the waiting list for liver transplantation [11]. However, there is a significant shortage of available donor livers. In 2022, only 9,528 liver

[1]Corresponding author (hvalidi@ttu.edu)

transplants were performed in the U.S., leaving a considerable gap between available livers and patients in need.

The United Network for Organ Sharing (UNOS) is responsible for overseeing organ allocation policies in the United States. For decades, the U.S. transplant allocation policy divided the nation into 11 geographical regions, which were further subdivided into 58 Donation Service Areas (DSAs). A DSA is a geographic area containing one or more transplant centers and donor hospitals. Each DSA is managed by an Organ Procurement Organization (OPO) responsible for recovering organs from deceased donors for transplantation in the U.S. Currently, the U.S. has 56 OPOs. Figure 1 illustrates all the current DSAs of the U.S. and their corresponding OPOs.

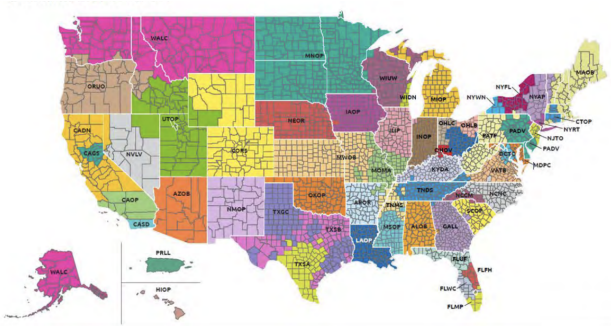

Figure 1: 56 DSAs of the U.S. (Image credit: `https://optn.transplant.hrsa.gov/media/3104/kidney_publiccomment_201908.pdf`)

Until recently, the Share 35 policy allocated livers to candidates based on the Model for End-stage Liver Disease (MELD) score, and candidates with MELD scores between 15 and 35 inside the DSA of an OPO were prioritized over those outside of the DSA. Because the Share 35 policy offered deceased donor livers hierarchically by prioritizing the candidates in the OPO's DSA, it faced criticism for creating disparities. Each region contained specific DSAs that share and receive livers reciprocally. In other words, sharing-and-receiving occurs only between the DSAs of the same region.

There are multiple reciprocal-based MIP formulations for the liver region redesign problem in the literature. Stahl et al. [10] introduce a bi-objective (i.e., efficiency and geographical equity) MIP to find an optimal configuration of liver transplant regions. Kong et al. [6] propose a branch-and-price approach for region design of the liver allocation system in the U.S. Demirci et al. [3] consider both objective functions of Stahl et al. [10] simultaneously

and develop a branch-and-price approach to solve larger instances of the problem. Gentry et al. [4] propose a MIP model to minimize the sum of absolute differences between the number of deceased-donor livers recovered in each district by partitioning the set of DSAs into a fixed number of districts.

Motivated by (i) reducing pre-transplant deaths, (ii) increasing pediatric transplantation, and (iii) reducing geographic variation in medical urgency scores at the time of transplant, UNOS currently implements an Acuity Circle policy, which considers fixed distance from the donor hospitals [12]. In this policy, the organs are shared incrementally in fixed-radius circles around donation locations.

The reciprocal approach raises concerns about geographic equity because the availability of and demand for donor livers can vary significantly from one region to another. To improve geographic equity and allow broader sharing, Kilambi and Mehrotra [5] introduced a neighborhood framework that is a hypothetical case in which sharing is not reciprocal. Following the neighborhood framework of Kilambi and Mehrotra [5], Akshat et al. [2] propose two two-phase mixed integer programming (MIP) formulations based on the neighborhood framework.

The neighborhood framework approach assigns, for each DSA, a sharing neighborhood and a receiving neighborhood, where it can share livers with the former and receive livers from the latter. Each neighborhood needs to form a contiguous region. Crucially, sharing and receiving in a neighborhood is not necessarily reciprocal, meaning that a DSA might share its livers with another DSA but receive no livers in return. The resulting neighborhoods may also overlap; in other words, a DSA might be in multiple other DSAs' sharing (receiving) neighborhoods. According to Akshat et al. [2], their circular contiguity model results in neighborhoods that enjoy the narrowest range of supply-demand ratios (≤ 0.15) in comparison with the models of Gentry et al. [4] (0.17) and Kilambi and Mehrotra [5] (0.64). Figure 2 illustrates the difference between a district/region-based and a neighborhood-based allocation solution on a 3×3 grid graph.

In the first formulation of Akshat et al. [2], contiguity is defined by the geographical connectivity of regions and is enforced using flow-based contiguity constraints. In the second formulation, circular contiguity is used to construct neighborhoods. These MIP models determine optimal allocations of livers from donor hospitals to transplant centers with respect to a fairness criterion in different transplantation centers and DSAs by maximizing the minimum supply-demand ratio among transplant centers. We refer the

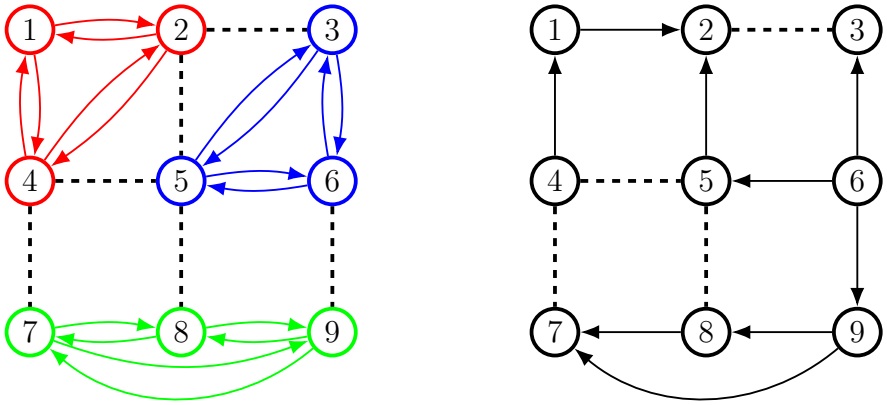

Figure 2: District-based and neighborhood-based strategies: (left) sharing-and-receiving of organs is allowed *only* in a district and it is reciprocal; (right) sharing-and-receiving of organs (not necessarily reciprocal) follows no specific rule.

reader to Akshat et al. [2] for more information about fairness in liver region redesign.

Motivated by the importance of the liver region redesign problem and computational challenges in solving the MIP formulations of Akshat et al. [2], we revisit the MIP formulations and propose new formulations that are at least as strong as the existing ones. Specifically, one of our proposed formulations solves a real-world instance of the problem in a matter of seconds, while a relaxation of an existing formulation of Akshat et al. [2] does not solve the problem to optimality after two hours.

Our Contributions

1. We provide stronger alternate MIP formulations for the flow model of Akshat et al. [2];

2. We propose stronger new MIP formulations for the circular model of Akshat et al. [2];

3. We conduct a polyhedral study on the circular model; and

4. We conduct computational experiments on real-world datasets, which results in solving multiple unsolved instances of the problem to optimality.

2. Preliminaries

2.1. Notation

For clarity, we employ the same notation used by Akshat et al. [2]. Let $\mathcal{I}$ and $\mathcal{J}$ be the set of supply and demand locations with sizes $\mathrm{N_{sup}}$ and $\mathrm{N_{dem}}$, respectively. Depending on the context, a supply location can be a DSA or a donor hospital. Furthermore, a demand location can be a DSA or a transplant center. For every supply location $i \in \mathcal{I}$, supply s_i denotes the number of recovered livers from deceased donors. For every demand location $j \in \mathcal{J}$, demand d_j denotes the number of patients on the waiting list. For every supply location $i \in \mathcal{I}$ and every demand location $j \in \mathcal{J}$, τ_{ij} denotes the distance (in nautical miles) between them. Furthermore, $\tau_{\max}$ represents the maximum allowable distance between supply and demand locations. For every demand location $j \in \mathcal{J}$, c_j denotes the number of its transplant centers. The minimum number of transplant centers that need to be covered by a supply location is denoted by $c_{\min}$. In both models, the minimum and maximum supply-to-demand ratios are denoted by λ and β, respectively.

2.2. Mathematical Models

Two mathematical models (phases) are discussed for each policy. Phase 1 maximizes the minimum ratio of total supplies supporting each demand location over the total demand of the demand location. The intuition behind the phase 1 model is provided below.

$$\begin{aligned}
&\max\ \lambda \\
&\sum_{i \in \mathcal{I}} \frac{\text{supply of location } i \text{ for demand location } j}{\text{total demand satisfied by location } i} \geq \lambda \qquad \forall j \in \mathcal{J} \\
&\text{other constraints.}
\end{aligned}$$

Phase 2 minimizes the maximum of the aforementioned ratio while the optimal objective obtained in phase 1 is respected as a lower bound of the ratio. In better words, the disparity between the best and the worst demand locations is minimized in phase 2 while the maximum supply-to-demand ratio obtained by the MIP model of phase 1 is respected [2]. Let λ^* be the best objective value obtained by solving phase 1. The intuition behind phase 2

model is provided below.

$$\min \ \beta$$

$$\lambda^* \leq \sum_{i \in \mathcal{I}} \frac{\text{supply of location } i \text{ for demand location } j}{\text{total demand satisfied by location } i} \leq \beta \qquad \forall j \in \mathcal{J}$$

other constraints.

2.3. Computational Setup and Data

Our computational experiments are conducted on a PC with an Intel Core i7-10750H CPU at 60GHz, using a 6-core with 16GB RAM. We employ Python 3.10.7 for coding and Gurobi 10.0.2 for solving the MIP models with a time limit of 3,600 seconds. As we are dealing with fractional objective values (supply-to-demand ratios), a MIP gap of 1% yields optimal objective values with two digits of precision that is acceptable in this context. So, we set the MIP gap to 1% in our computational results. We note that Akshat et al. [2] set the MIP gap to 0.01% (Gurobi's default gap), and we follow their MIP gap setting when we are comparing our results with theirs in Sections 3.2 and 3.3. We consider two sets of liver transplantation data for running our experiments: (i) data from July 2013 to June 2017 (DATASET1), and (ii) data from January 2018 to December 2022 (DATASET2). DATASET1 is obtained by requesting the data from the first author of Akshat et al. [2], and DATASET2 is obtained by requesting data from the Organ Procurement & Transplantation Network website at `https://optn.transplant.hrsa.gov/data/view-data-reports/request-data/`. We note that DATASET1 does not contain data needed for running experiments with the Acuity Circle policy models. Code, data and results for DATASET2 are available at `https://github.com/Alpha-kun/Stronger_MIP_Formulations_for_the_Liver_Region_Redesign_Problem`.

We use the total number of registered patients on the waitlist to represent the demand for a transplant center (DSA) and the number of cadaverous livers provided by a donor hospital (DSA) to represent the supply of the hospital (DSA). For the Acuity Circle policy, we used $\tau_{\max}$ that ranges from 450-750nm, with an increment of 50nm, while for the Share 35 policy, $\tau_{\max}$ ranges from 500-700nm, with a step size of 100nm where nm stands for Nautical Miles. For Acuity Circle models, we set $c_{min} = 3$ to ensure each donor hospital will share organs with at least 3 different transplant centers. This is consistent with the value of c_{min} in Akshat et al. [2]. Furthermore,

we consider a new radius for any demand location around a supply location.

We consider two setups for our computational experiments: (i) a setup with the supply and demand sets as the set of DSAs (SETUP1), and (ii) a setup with the supply set of 3-digit zip codes[2] and the demand set of transplantation centers (SETUP2). For the 3-digit zip codes, we group donor hospitals if their 5-digit zip codes share the same three-digit prefix (See Akshat et al. [2] for a similar approach). We note that the numbers of DSAs and 3-digit zip codes are 58 and 677, respectively, and the number of transplant centers is 149. The location of each hospital is denoted by its latitude and longitude, and the location of a cluster of hospitals is determined by taking the average of their locations. We employ the Vincenty method the GeoPy package implements to compute the distance between a cluster and a transplant center [1]. For the Acuity Circle policy, we exclude the supply and demand locations of Hawaii, Puerto Rico, and the Virgin Islands, as even the maximum value $\tau_{\max}$ (i.e., $\tau_{\max} = 700$ nm) cannot cover any part of the mainland U.S.

3. Liver Allocation Models with Flow-based Contiguity

In this section, we (i) provide the MIP models of Akshat et al. [2] with flow-based contiguity, (ii) propose a stronger alternate MIP formulation, and (iii) conduct a set of computational experiments. For every supply location $i \in \mathcal{I}$ and every demand location $j \in \mathcal{J}$, decision variable x_{ij} is one if location i shares organs with location j and zero otherwise.

3.1. Flow Models of Akshat et al. [2]

The MIP model of the first phase is provided as follows. This model maximizes the minimum ratio of supply-to-demand among all demand locations.

[2]Due to the space limitation, our computational results for 4-digit zip codes are available on GitHub.

$$\max\ \lambda \tag{1a}$$

$$\sum_{i\in\mathcal{I}} \frac{1}{\sum_{k\in\mathcal{J}} d_k x_{ik}} s_i x_{ij} \geq \lambda \qquad \forall j \in \mathcal{J} \tag{1b}$$

$$\sum_{j\in\mathcal{J}} c_j x_{ij} \geq c_{\min} \qquad \forall i \in \mathcal{I} \tag{1c}$$

$$x_{ii} = 1 \qquad \forall i \in \mathcal{I} \tag{1d}$$

$$\tau_{ij} x_{ij} \leq \tau_{max} \qquad \forall i \in \mathcal{I}, j \in \mathcal{J} \tag{1e}$$

$$x_{ij} \in \{0,1\} \qquad \forall i \in \mathcal{I}, j \in \mathcal{J}. \tag{1f}$$

Objective function (1a) maximizes the minimum ratio of supply-to-demand (see λ in constraints (1b)) among all demand locations. Constraints (1c) enforce that every supply location must cover at least c_{min} transplant centers. Constraints (1d) imply that a supply location satisfies its demand if it is a demand location as well. Constraints (1e) imply that a supply location cannot share its organs with a demand location if the distance between them is more than τ_{max}. We note that a linearized variant of constraints (1b) is available in Appendix B of Akshat et al. [2].

As contiguity is not imposed by formulation (1), one needs to add contiguity constraints because they capture a notion of compactness [2]. An area is contiguous if one can move from one point of it to another point without leaving the area. Akshat et al. [2] employ the flow-based contiguity constraints of Shirabe [8, 9] for imposing contiguity. Let $G = (V, E)$ be a graph in which the vertex set V represents the set of locations and the edge set E denotes the edges that connect adjacent pairs. We define A as the bidirected variant of the edge set E (i.e., every edge $\{u, v\} \in E$ corresponds to arcs (u, v) and (v, u) in A.) Furthermore, m_1 (m_2) can be defined as the maximum number of supply (demand) locations that can be assigned to a demand (supply) location [2]. One can define $m_1 := |\mathcal{I}|$ and $m_2 := |\mathcal{J}|$. For every vertex $v \in V$, set $N(v)$ denotes the open neighborhood of vertex v. For every demand location $j \in J$ (supply location $i \in I$) and every arc $(u, v) \in A$, decision variable f^j_{uv} (g^i_{uv}) denotes the flow of type j (i) on arc (u, v). Constraints (2) and (3) are the receiving and sharing contiguity

constraints, respectively.

$$\sum_{k\in N(i)} f^j_{ik} - \sum_{k\in N(i)} f^j_{ki} = x_{ij} \quad \forall i \in \mathcal{I}\setminus\{j\},\ \forall j \in \mathcal{J} \tag{2a}$$

$$\text{(Receiving)} \quad \sum_{k\in N(j)} f^j_{jk} = 0 \quad \forall j \in \mathcal{J} \tag{2b}$$

$$\sum_{k\in N(i)} f^j_{ki} \le (m_1 - 1)x_{ij} \quad \forall i \in \mathcal{I},\ \forall j \in \mathcal{J}. \tag{2c}$$

$$\sum_{k\in N(j)} g^i_{jk} - \sum_{k\in N(j)} g^i_{kj} = x_{ij} \quad \forall i \in \mathcal{I}\setminus\{j\},\ \forall j \in \mathcal{J} \tag{3a}$$

$$\text{(Sharing)} \quad \sum_{k\in N(i)} g^i_{ik} = 0 \quad \forall i \in \mathcal{I} \tag{3b}$$

$$\sum_{k\in N(j)} g^i_{kj} \le (m_2 - 1)x_{ij} \quad \forall i \in \mathcal{I},\ \forall j \in \mathcal{J}. \tag{3c}$$

Constraints (2a) (constraints (3a)) imply that if supply location $i \in \mathcal{I}$ shares organs with demand location $j \in \mathcal{J}$, then a flow of type j (type i) must leave supply location i (demand location j). Constraints (2b) (constraints (3b)) imply that no flow of type j (type i) is sent out from demand location j (supply location i). Constraints (2c) (constraints (3c)) imply that if a supply location $i \in \mathcal{I}$ shares no organ with a demand location $j \in \mathcal{J}$, then Then no flow of type j (type i) can pass the supply location i (demand location j).

An illustration of sharing and receiving contiguity is shown in Figure 3.

Let λ^* be the best objective value of the first phase model (1) that maximizes the minimum ratio of supply-to-demand among all demand locations. Now we provide Akshat et al. [2]'s second phase MIP model.

$$\min\ \beta \tag{4a}$$

$$\lambda^* \le \sum_{i\in\mathcal{I}} \frac{1}{\sum_{k\in\mathcal{J}} d_k x_{ik}} s_i x_{ij} \le \beta \quad \forall j \in \mathcal{J} \tag{4b}$$

$$\text{constraints (1c)-(1f).} \tag{4c}$$

Objective function (4a) minimizes the difference between supply-to-demand ratios by minimizing the maximum ratio of supply-to-demand (see constraints

(a) Receiving contiguity (b) Sharing contiguity

Figure 3: An illustration of receiving and sharing contiguity: if a transplant center (donor hospital) receives (shares) livers from (to) a non-neighbor donor hospital (transplant center), then it should be able to receive (share) livers via a path containing donor hospitals (transplant centers).

(4b)) among all demand locations.

3.2. New Models with Cut-based Contiguity

Due to the recent successful performance of contiguity cutting planes in the districting context [13], we propose similar cutting planes for imposing receiving and sharing contiguity constraints. While Akshat et al. [2] report a MIP gap of 1.19% for the first phase of the flow model with only sharing contiguity constraints (3) after two hours, we show that the contiguity cutting planes provide optimal solutions in a matter of seconds when both sharing and receiving contiguity constraints are imposed, and the MIP gap is set to 0.01% (similar to the MIP gap of Akshat et al. [2]). We note that the specifications of Akshat et al. [2]'s machine are superior to ours detailed in Section 2.3.

Definition 1 (Validi et al. [13]). A subset $C \subseteq V \setminus \{a, b\}$ of vertices is an a, b-separator for $G = (V, E)$ if there is no path from a to b in $G - C$.

For every non-adjacent pair of vertices $\{a, b\} \in \binom{V}{2}$ and every a, b-separator C, denoted by (a, b, C), the receiving and sharing contiguity constraints are as follows.

$$x_{ab} \leq \sum_{c \in C} x_{cb} \qquad \forall (a, b, C) \qquad \text{(5a)}$$

$$x_{ab} \leq \sum_{c \in C} x_{ac} \qquad \forall (a, b, C) \qquad \text{(5b)}$$

Figure 4 shows an illustration of receiving and sharing a, b-separator inequalities. Let $\mathcal{P}_f^i$ and $\mathcal{P}_c^i$ be the set of the continuous relaxations of models in phase i ($i \in \{1, 2\}$) with flow-based and cut-based contiguity constraints, respectively. Then, the following proposition provides a comparison between these sets.

Proposition 1 (cf. Theorem 1 of Validi et al. [13]). For either phase $i \in \{1, 2\}$, we have $\mathcal{P}_c^i \subseteq \mathcal{P}_f^i$ and this can be strict.

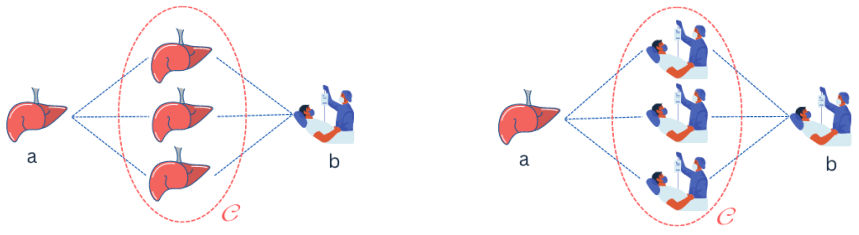

(a) $x_{ab} \leq \Sigma_{c \in \mathcal{C}} x_{cb}$ (b) $x_{ab} \leq \Sigma_{c \in \mathcal{C}} x_{ac}$

Figure 4: An illustration of a, b-separator inequalities: (a) receiving a, b-separator inequalities; (b) sharing a, b-separator inequalities.

As we have exponentially many constraints of types (5a) and (5b), we need to add them on-the-fly; i.e., we need to find violated inequalities as we proceed in the branch-and-cut tree. Fortunately, it is easy to find violated inequalities when we encounter integral infeasible solutions. In better words, the integer separation problems corresponding to inequalities (5a) and (5b) are polynomially solvable. For more technical details of the integer separation algorithm, interested readers are encouraged to see Algorithm 1 of Validi et al. [13]. We note that lines 7-10 of their algorithm are unnecessary in our case.

3.3. Computational Results

We run our experiments as described in Section 2.3. We note that a best solution of phase 1's model is feasible for phase 2's. So, we employ a best solution of phase 1 as a heuristic to warm start the second phase model. Our initial computational experiments showed that this problem gets more challenging as the value of $\tau_{\max}$ increases. To alleviate this issue, we adopt the following warm start strategy: any MIP formulation with $\hat{\tau}_{\max}$ is warm started with a solution of a MIP formulation with $\bar{\tau}_{\max}$, where $\bar{\tau}_{\max} < \hat{\tau}_{\max}$. For example, a MIP formulation with $\tau_{\max} = 700$ nm can be warm started by

a solution of a MIP model with $\tau_{\max} = 600$ nm, which can be further warm started by a solution of a MIP model with $\tau_{\max} = 500$. As the MIPs for both phases are nonlinear, we linearized them based on Appendix B of Akshat et al. [2].

Table 1 summarizes our computational results under DATASET1 and SETUP1. In this table, column "$\tau_{\max}$ (contig.)" shows the $\tau_{\max}$ value and contiguity constraint type (i.e., flow or cut). Columns "Best incumbent" and "Best bound" denote the best feasible solution and best bounds obtained by solving the MIP formulations after an hour. As we always warm start the MIP of phase 2 with the best feasible solution of phase 1, we use "-" under the column of "w/o heur." (i.e., without heuristic) for any row of type phase 2. Furthermore, we set "NA" for any crossing of phase 1 for "$\tau_{\max} = 500$ nm and column "w/heur." (i.e., with heuristic) because $\tau_{\max} = 500$ nm is the smallest $\tau_{\max}$ for these models and no feasible solution is available for its corresponding MIP model in phase 1. Column "B&B (#)" denotes the number of explored branch-and-bound nodes in 3,600 seconds. Finally, column "Gap in % (time in sec.)" denotes either an optimality gap or solving time within the 1-hour time limit.

For $\tau_{\max} = 500$ nm, Akshat et al. [2] report an optimality gap of 1.19% after two hours of running their flow-based model with only sharing contiguity constraints, while we report an optimality gap of 0.18 % for our implementation of the flow-based model with both sharing and receiving contiguity constraints when the MIP gap is set to 0.01%, which is the Gurobi's MIP gap default. Our computational results show that our cut-based model solves the problem in 35 seconds with the same default gap. Since we have fractional objective values (supply-to-demand ratios), a MIP gap of 1% is acceptable and yields optimal objectives with two digits of precision. Table 1 shows the flow-based model can solve the problem when the MIP gap is set to 1%. We observe that both phases of the MIP model are solved when $\tau_{\max} \in \{600, 700\}$ nm while we struggle to solve the second phase of the MIP model for $\tau_{\max} = 500$ nm. Although the cut-based models are at least as strong as the flow-based models, Table 1 shows the superiority of the compact flow-based models in practice. This observation can be explained by the fact that the reduced cost fixing procedure is disabled when the `callback` feature of Gurobi is active for adding contiguity cutting planes on the fly. Figure 5 demonstrates a liver allocation map of the U.S. at the DSA level when $\tau_{\max} = 700$ nm. Due to the space limitation, the results under DATASET2 and SETUP1 are reported in Appendix B.

Table 1: Computational results for the MIP formulations with flow- and cut-based contiguity under DATASET1 and SETUP1 within a time limit of 3,600 seconds and MIP gap of 1%

τ_{max} (contig.)	Phase	Best incumbent		Best bound		B&B (#)		Time in sec. (gap in %)	
		w/o heur.	w/ heur.	w/o heur.	w/ heur.	w/o heur.	w/ heur.	w/o heur.	w/ heur.
500 (flow)	1	0.57	NA	0.57	NA	5,790	NA	10	NA
	2	-	0.71	-	0.70	-	186,264	-	(1.12)
500 (cut)	1	0.57	NA	0.58	NA	54,504	NA	30	NA
	2	-	0.71	-	0.70	-	398,957	-	(1.45)
600 (flow)	1	0.61	0.61	0.61	0.61	2,971	4,658	18	30
	2	-	0.70	-	0.69	-	64,626	-	2,042
600 (cut)	1	0.61	0.61	0.61	0.61	57,336	122,222	64	145
	2	-	0.70	-	0.69	-	259,961	-	(1.28)
700 (flow)	1	0.61	0.61	0.61	0.61	6,102	0	78	1
	2	-	0.70	-	0.69	-	25,903	-	1,707
700 (cut)	1	0.61	0.61	0.61	0.61	79,088	0	132	0
	2	-	0.71	-	0.69	-	229,016	-	(2.28)

Figure 5: A liver sharing network map of the U.S. with $\tau_{\max} = 700$ nm

4. Liver Allocation Models with Circular Contiguity

Akshat et al. [2]'s models with circular contiguity are similar to a set partitioning formulation in which (i) each supply location must be assigned to exactly one coverage radius in a specific range and (ii) circular contiguity is imposed. Mehrotra et al. [7] employed a similar radius-bounded strategy

for designing compact political districts whose radius from a center is at most three hops. Unlike the flow models (1) and (4), this is a linear model in both phases one and two. For every supply location $i \in \mathcal{I}$, we define R_i as the set of radius values the supply location can cover. For every supply location $i \in \mathcal{I}$ and every radius $r \in R_i$, (i) c_i^r denotes the number of transplant centers that are at most r units away from the supply location i, and (ii) binary decision variable x_{ir} is one if supply location i covers demand locations in a distance of at most r units from the supply location i. In our computational experiments, we define a new radius for every demand location around a supply location. This approach is similar to that of Akshat et al. [2].

4.1. Circular Models of Akshat et al. [2]

The model of the first phase, which maximizes the minimum supply-to-demand ratio among all demand locations, is provided below.

$$\max \ \lambda \tag{6a}$$

$$\sum_{i\in\mathcal{I}} \sum_{r\in R_i:\tau_{ij}\le r} \frac{s_i}{\sum_{k:\tau_{ik}\le r} d_k} x_{ir} \ge \lambda \qquad \forall j \in \mathcal{J} \tag{6b}$$

$$\sum_{r\in R_i} x_{ir} = 1 \qquad \forall i \in \mathcal{I} \tag{6c}$$

$$\sum_{r\in R_i} c_i^r x_{ir} \ge c_{\min} \qquad \forall i \in \mathcal{I} \tag{6d}$$

$$x_{ir} \in \{0,1\} \qquad \forall r \in R_i, i \in \mathcal{I}. \tag{6e}$$

Objective function (6a) maximizes the minimum supply-to-demand ratio (see constraints (6b)) among all demand locations. Constraints (6c) imply that every supply location $i \in I$ must be assigned to exactly one covering radius $r \in R_i$. Constraints (6d) imply that every supply location must cover at least c_{min} transplant centers.

Let n' be the number of x variables in model (6). We define the linear programming (LP) relaxation set of formulation (6) as follows.

$$\mathcal{P}_1 := \{(x,\lambda) \in \mathbb{R}_+^{n'} \times \mathbb{R} \mid (x,\lambda) \text{ satisfies constraints (6b)-(6d)}\}.$$

Let λ^* be the best objective value of the first phase model (6). The second phase model, which seeks to minimize the disparity between supply-

to-demand ratios, is provided below.

$$\min \ \beta \tag{7a}$$

$$\lambda^* \leq \sum_{i \in \mathcal{I}} \sum_{r \in R_i : \tau_{ij} \leq r} \frac{s_i}{\sum_{k:\tau_{ik} \leq r} d_k} x_{ir} \leq \beta \qquad \forall j \in \mathcal{J} \tag{7b}$$

$$\text{Constraints (6c)-(6e).} \tag{7c}$$

Objective function (7a) minimizes the difference between supply-to-demand ratios (see constraints (7b)) among demand locations. We define the LP relaxation set of formulation (7) as follows.

$$\mathcal{P}_2 := \{(x, \lambda) \in \mathbb{R}_+^{n'} \times \mathbb{R} \mid (x, \lambda) \text{ satisfies constraints (7b) and (6c)-(6d)}\}.$$

4.2. New Models with Circular Contiguity and Polyhedral Studies

We propose a set of variable fixing for the model with circular contiguity. For every supply location $i \in \mathcal{I}$, we consider the following model in the first phase. This model maximizes the supply-to-demand ratio for every supply location such that (i) the supply location is assigned to exactly one radius, and (ii) the supply location covers at least c_{min} transplant centers.

$$\max \ z_i = \sum_{r \in R_i} \frac{s_i}{\sum_{k:\tau_{ik} \leq r} d_k} x_{ir} \tag{8a}$$

$$\sum_{r \in R_i} x_{ir} = 1 \tag{8b}$$

$$\sum_{r \in R_i} c_i^r x_{ir} \geq c_{\min} \tag{8c}$$

$$x_{ir} \in \{0, 1\} \qquad \forall r \in R_i. \tag{8d}$$

As model (8) seeks to find the smallest $r \in R_i$ such that (8c) holds, the following remark shows that it is polynomially solvable.

Remark 1. For every supply location $i \in \mathcal{I}$, MIP model (8) is solvable in $O(|R_i|)$ time.

For every supply location $i \in \mathcal{I}$, let z_i^* and $r_i^* \in R_i$ be the optimal objective value and the optimal radius obtained by solving MIP model (8) to optimality, respectively. For every supply location $i \in \mathcal{I}$ and every demand

location $j \in \mathcal{J}$, we define $\hat{\lambda}_{ij}$ as follows.

$$\hat{\lambda}_{ij} = \begin{cases} z_i^* & \text{if } \tau_{ij} \leq r_i^*, \\ 0 & \text{otherwise.} \end{cases}$$

For any demand location $j \in \mathcal{J}$, we define $\hat{\lambda}_j = \sum_{i \in I} \hat{\lambda}_{ij}$. Furthermore, we define $\bar{R}_i$ as follows.

$$\bar{R}_i = \{r \in R_i : r > r_i^*\}.$$

For every demand location $j \in \mathcal{J}$, we define $\mathcal{I}_j$ as follows.

$$\mathcal{I}_j = \{i \in \mathcal{I} : \tau_{ij} \leq \tau_{\max}\}.$$

Now, we propose the reduced model of phase 1 as follows.

$$\max \ \lambda \tag{9a}$$

$$\lambda \leq \sum_{i \in \mathcal{I}_j} \sum_{r \in \bar{R}_i : \tau_{ij} \leq r} \frac{s_i}{\sum_{k:\tau_{ik} \leq r} d_k} x_{ir} + \sum_{i \in \mathcal{I}_j} \hat{\lambda}_{ij} \Big(1 - \sum_{r \in \bar{R}_i : \tau_{ij} \leq r} x_{ir}\Big) \qquad \forall j \in \mathcal{J} \tag{9b}$$

$$\sum_{r \in \bar{R}_i} x_{ir} \leq 1 \qquad \forall i \in \mathcal{I} \tag{9c}$$

$$x_{ir} \in \{0,1\} \qquad \forall r \in \bar{R}_i, i \in \mathcal{I}. \tag{9d}$$

We also note that a constraint of type (9c) is redundant for any supply location $i \in \mathcal{I}$ with $|\bar{R}_i| = 1$. Furthermore, constraints (9b) can be simplified as follows.

$$\lambda \leq \hat{\lambda}_j + \sum_{i \in \mathcal{I}_j} \sum_{r \in \bar{R}_i : \tau_{ij} \leq r} \Big(\frac{s_i}{\sum_{k:\tau_{ik} \leq r} d_k} - \hat{\lambda}_{ij}\Big) x_{ir} \qquad \forall j \in \mathcal{J}. \tag{10}$$

Let n be the number of x variables in model (9). Now we define the LP relaxation set of the reduced model in phase 1 as follows.

$$\mathcal{P}_{R1} := \{(x, \lambda) \in \mathbb{R}_+^n \times \mathbb{R} \mid (x, \lambda) \text{ satisfies constraints (9c) and (10)}\}.$$

Let λ^* be the best objective value of model (9). Then the model of phase 2

can be written as follows.

$$\min\ \beta \tag{11a}$$

$$\sum_{i\in\mathcal{I}_j}\sum_{r\in\bar{R}_i:\tau_{ij}\le r}\frac{s_i}{\sum_{k:\tau_{ik}\le r}d_k}x_{ir}+\sum_{i\in\mathcal{I}_j}\hat{\lambda}_{ij}\Big(1-\sum_{r\in\bar{R}_i:\tau_{ij}\le r}x_{ir}\Big)\le\beta \qquad \forall j\in\mathcal{J} \tag{11b}$$

$$\sum_{i\in\mathcal{I}_j}\sum_{r\in\bar{R}_i:\tau_{ij}\le r}\frac{s_i}{\sum_{k:\tau_{ik}\le r}d_k}x_{ir}+\sum_{i\in\mathcal{I}_j}\hat{\lambda}_{ij}\Big(1-\sum_{r\in\bar{R}_i:\tau_{ij}\le r}x_{ir}\Big)\ge\lambda^* \qquad \forall j\in\mathcal{J} \tag{11c}$$

$$\sum_{r\in\bar{R}_i}x_{ir}\le 1 \qquad \forall i\in\mathcal{I} \tag{11d}$$

$$x_{ir}\in\{0,1\} \qquad \forall r\in\bar{R}_i, i\in\mathcal{I}. \tag{11e}$$

Now we define the LP relaxation set of the reduced model in phase 2 as follows.

$$\mathcal{P}_{R2}:=\{(x,\beta)\in\mathbb{R}^n_+\times\mathbb{R}\mid (x,\beta)\text{ satisfies constraints (11b)-(11d)}\}.$$

Now, we propose polyhedral results on the Acuity Circle policy models.

Lemma 1. Polyhedron $\mathcal{P}_{R1}$ is full-dimensional.

Proof. We note that points (i) $(\mathbf{0},0)\in\mathcal{P}_{R1}$, (ii) unit vector $(e_v,0)\in\mathcal{P}_{R1}$ for every $v\in[n]$, and (iii) $(\mathbf{0},\min_{j\in J}\{\hat{\lambda}_j\})\in\mathcal{P}_{R1}$. It is easy to see that these points form $n+2$ affinely independent points. So, $\mathcal{P}_{R1}$ is a full-dimensional polyhedron. □

Proposition 2. Packing constraints (9c) induce facets for polyhedron $\mathcal{P}_{R1}$.

Proof. As $\mathcal{P}_{R1}$ is full-dimensional by Lemma 1, it suffices to find $n+1$ affinely independent points that satisfy constraints (9c) at equality. Let $i\in\mathcal{I}$ be a supply location. For every radius $r\in\bar{R}_i$, let point $(e_{ir},0)\in\mathcal{P}_{R1}$ be the unit vector with 1 for x_{ir} and 0 for other elements. Then, we define $P_1=\{(e_{ir},0)|r\in\bar{R}_i\}$. Furthermore, we fix r' as an arbitrary radius belonging to $\bar{R}_i$. Then, we define $P_2=\{(e_{jr}+e_{ir'},0)|j\in\mathcal{I}\setminus\{i\},\ r\in\bar{R}_j\}$. Finally, we define point $q:=(e_{ir'},\min_{j\in\mathcal{J}}\{\hat{\lambda}_j+\frac{s_i}{\sum_{k:\tau_{ik}\le r'}d_k}-\hat{\lambda}_{ij}\})$ with r' be a radius that belongs to $\bar{R}_i$. We note that $q\in\mathcal{P}_{R1}$. Points of the set $P_1\cup P_2\cup\{q\}$ form $n+1$ affinely independent points and satisfy inequalities (9c) for supply location $i\in\mathcal{I}$ at equality (see Table 2 in Appendix A). □

We conclude this section by providing two results that show the reduced circular MIP models are at least as strong as the existing ones.

Theorem 1. $\mathcal{P}_{R1} \subseteq \operatorname{proj} \mathcal{P}_1$ with $\operatorname{proj} \mathcal{P}_1$ be a projection of $\mathcal{P}_1$ after the variable fixing procedure.

Proof. Let $(\bar{x}, \bar{\lambda})$ be a point that belongs to polyhedron $\mathcal{P}_{R1}$. We are to show that there exists point $(\hat{x}, \bar{\lambda})$ that belongs to $\mathcal{P}_1$. For every binary variable x_{ir} that exists in both models (6) and (9) (i.e., for every supply location $i \in \mathcal{I}$ and every radius $r \in \bar{R}_i$), we set $\hat{x}_{ir} := \bar{x}_{ir}$. For every supply location $i \in \mathcal{I}$, let r_i^* be the index for the largest radius in $R \setminus \bar{R}_i$. We set $\hat{x}_{ir_i^*} = 1 - \sum_{r \in \bar{R}_i} \bar{x}_{ir}$. For every supply location $i \in \mathcal{I}$ and every radius index $r \in (R \setminus \bar{R}_i) \setminus \{r_i^*\}$, we set $\hat{x}_{ir} = 0$. This implies that $(\hat{x}, \bar{\lambda})$ satisfies constraints (6c).

Now, we show that $(\hat{x}, \bar{\lambda})$ satisfies constraints (6d).

$$\sum_{r \in R_i} c_i^r \hat{x}_{ir} = \sum_{r \in \bar{R}_i} c_i^r \hat{x}_{ir} + c_i^{r_i^*} \hat{x}_{ir_i^*} \geq c_i^{r_i^*} \geq c_{\min}.$$

Finally, we show that $(\hat{x}, \bar{\lambda})$ satisfies constraints (6b).

$$\begin{aligned}
\sum_{i \in \mathcal{I}_j} \sum_{r \in R_i : \tau_{ij} \leq r} \frac{s_i}{\sum_{k : \tau_{ik} \leq r} d_k} \hat{x}_{ir} &= \sum_{i \in \mathcal{I}_j} \sum_{r \in \bar{R}_i : \tau_{ij} \leq r} \frac{s_i}{\sum_{k : \tau_{ik} \leq r} d_k} \hat{x}_{ir} \\
&\quad + \sum_{i \in \mathcal{I}_j} \hat{\lambda}_{ij} \hat{x}_{ir_i^*} \\
&= \sum_{i \in \mathcal{I}_j} \sum_{r \in \bar{R}_i : \tau_{ij} \leq r} \frac{s_i}{\sum_{k : \tau_{ik} \leq r} d_k} \bar{x}_{ir} \\
&\quad + \sum_{i \in \mathcal{I}_j} \hat{\lambda}_{ij} (1 - \sum_{r \in \bar{R}_i : \tau_{ij} \leq r} \bar{x}_{ir}) \\
&\geq \bar{\lambda}.
\end{aligned}$$

Here, the second equality holds by the definition of $\hat{x}_{ir_i^*}$ for every supply location $i \in \mathcal{I}$. The last inequality holds by constraints (9b). □

Theorem 2. $\mathcal{P}_{R2} \subseteq \operatorname{proj} \mathcal{P}_2$ with $\operatorname{proj} \mathcal{P}_2$ be a projection of $\mathcal{P}_2$ after the variable fixing procedure.

Proof. The proof is similar to that of Theorem 1. □

We finally note that the number of fixed variables is exactly $c_{\min}|I|$ because we define a new radius for every demand location around a supply location in our computational experiments. This approach of creating radii

is consistent with that of Akshat et al. [2]. Depending on the $\tau_{\max}$ value, we fix roughly 4-7 % of binary decision variables in our computational experiments (the larger $\tau_{\max}$, the smaller fix percentage). We discuss the effect of the variable fixing procedure in Section 4.3.

4.3. Computational Results

In this set of experiments, we consider *only* SETUP2 as circular models can solve the instances of SETUP1 in less than one second. In our computational experiments, we recall that the number of fixed variables is exactly $c_{\min}|I|$, equal to $3 \times 677 = 2,031$. Figure 6 shows the effect of variable fixing for the first phase of circular MIP formulation (6). While the variable fixing procedure improves the optimality gap for $\tau_{\max} \in \{500, 600, 650\}$ in a time limit of one hour, it makes no/tiny difference for $\tau_{\max} \in \{450, 550\}$. Counterintuitively, the fixing procedure worsens the optimality gap for $\tau_{\max} = 700$ nm in the one-hour time limit. A detailed report of our computational experiments with the first and second phases of MIP formulations with circular contiguity (6) and (7) is provided in Appendix C. Finally, we note that we were not able to run our experiments under SETUP2 and DATASET1 as DATASET1, which is provided by Akshat et al. [2], does not contain the data needed for running computational experiments under SETUP2.

5. Conclusion and Future Work

This paper explores the existing MIP models of the liver region redesign problem with flow-based and circular contiguity. For the first formulation, we investigate a compact flow-based and a cut-based formulation with exponentially many constraints. We propose a variable fixing procedure for the formulation with circular contiguity that makes a set of constraints facet-defining. Our implementations of the MIP models solve multiple instances of the problem to optimality. As a future work, one may be interested in new approaches for handling the nonlinearity of the first formulation. Another interesting direction might be the managerial insights that one can provide for policymakers. Furthermore, our theoretical results can be employed in other applications like designing radius-bounded districting plans and telecommunication networks.

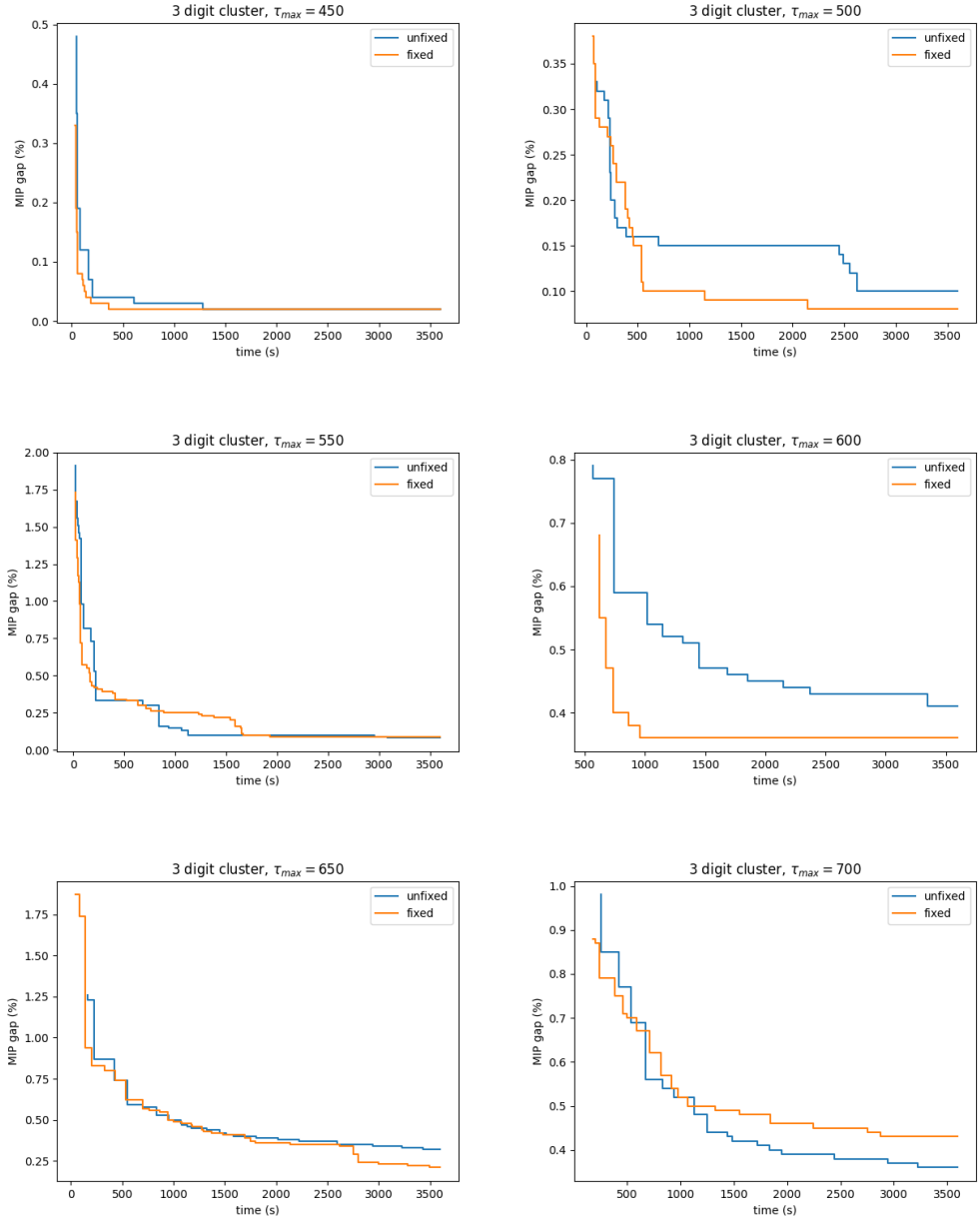

Figure 6: Effect of variable fixing on the optimality gap for the first phase of MIP formulation with circular contiguity (6) during a time limit of 3,600 seconds.

Disclaimer

DATASET2 reported here have been supplied by the United Network for Organ Sharing as the contractor for the Organ Procurement and Transplantation Network. The interpretation and reporting of these data are the responsibility of the author(s) and in no way should be seen as an the official policy of or interpretation by the OPTN or the U.S. Government.

Acknowledgement

This research was supported by Office of Naval Research grant N0001421 12262. We would like to thank the United Network for Organ Sharing for providing all data needed for the models with circular contiguity. We also thank Shubham Akshat of the Tepper School of Business at Carnegie Mellon University for sharing parts of the data from Akshat et al. [2] for running the models with flow- and cut-based contiguity.

References

[1] GeoPy's documentation. 2023.
URL `https://geopy.readthedocs.io/en/stable/index.html`

[2] Akshat, S., S. E. Gentry and S. Raghavan. Heterogeneous donor circles for fair liver transplant allocation. *Health Care Management Science*, 2022. doi:10.1007/s10729-022-09602-7.
URL `https://doi.org/10.1007/s10729-022-09602-7`

[3] Demirci, M. C., A. J. Schaefer, H. E. Romeijn and M. S. Roberts. An exact method for balancing efficiency and equity in the liver allocation hierarchy. *INFORMS Journal on Computing*, 24(2):260–275, 2012.

[4] Gentry, S., E. Chow, A. Massie and D. Segev. Gerrymandering for justice: redistricting US liver allocation. *Interfaces*, 45(5):462–480, 2015.

[5] Kilambi, V. and S. Mehrotra. Improving liver allocation using optimized neighborhoods. *Transplantation*, 101(2):350–359, 2017.

[6] Kong, N., A. J. Schaefer, B. Hunsaker and M. S. Roberts. Maximizing the efficiency of the us liver allocation system through region design. *Management Science*, 56(12):2111–2122, 2010.

[7] Mehrotra, A., E. L. Johnson and G. L. Nemhauser. An optimization based heuristic for political districting. *Management Science*, 44(8):1100–1114, 1998.

[8] Shirabe, T. A model of contiguity for spatial unit allocation. *Geographical Analysis*, 37(1):2–16, 2005.

[9] Shirabe, T. Districting modeling with exact contiguity constraints. *Environment and Planning B: Planning and Design*, 36(6):1053–1066, 2009.

[10] Stahl, J. E., N. Kong, S. M. Shechter, A. J. Schaefer and M. S. Roberts. A methodological framework for optimally reorganizing liver transplant regions. *Medical Decision Making*, 25(1):35–46, 2005.

[11] UNOS. Making liver distribution fair and equitable. 2023.
URL `https://unos.org/policy/liver/`

[12] UNOS. System notice: Liver and intestinal organ distribution based on acuity circles implemented Feb. 4. 2023.
URL `https://unos.org/news/system-implementation-notice-liver-and-intestinal-organ-distribution-based-on-acuity-circles-implemented-feb-4/`

[13] Validi, H., A. Buchanan and E. Lykhovyd. Imposing contiguity constraints in political districting models. *Operations Research*, 70(2):867–892, 2022.

Appendix A

Table 2: $n+1$ affinely independent points that satisfy inequalities (9c) for supply location $i \in \mathcal{I}$ at equality. For any $j \in \mathcal{I} \setminus \{i\}$, we define vector $x_{j,R_j} := (x_{j,1}, \cdots, x_{j,|\bar{R}_j|})^T$ because of space limitation.

	P_1					P_2							q
λ			$\mathbf{0}$			$\mathbf{0}$	$\mathbf{0}$	$\mathbf{0}$	$\mathbf{0}$	$\mathbf{0}$	$\mathbf{0}$	$\mathbf{0}$	$\min_{j\in\mathcal{J}}\{\hat{\lambda}_j + \frac{s_i}{\sum_{k:\tau_{ik}\le r'} d_k} - \hat{\lambda}_{ij}\}$
x_{1,R_1}			$\mathbf{0}$			$\mathbf{I}$	$\mathbf{0}$	$\mathbf{0}$	$\mathbf{0}$	$\mathbf{0}$	$\mathbf{0}$	$\mathbf{0}$	0
x_{2,R_2}			$\mathbf{0}$			$\mathbf{0}$	$\mathbf{I}$	$\mathbf{0}$	$\mathbf{0}$	$\mathbf{0}$	$\mathbf{0}$	$\mathbf{0}$	0
$\vdots$			$\vdots$			$\vdots$	$\ddots$	$\ddots$	$\ddots$	$\vdots$	$\vdots$	$\vdots$	$\vdots$
$x_{i-1,R_{i-1}}$			$\mathbf{0}$			$\mathbf{0}$	$\mathbf{0}$	$\mathbf{0}$	$\mathbf{I}$	$\mathbf{0}$	$\mathbf{0}$	$\mathbf{0}$	0
x_{i,r_1}	1	$\dots$	0	$\dots$	0	$\mathbf{0}$	$\mathbf{0}$	$\mathbf{0}$	$\mathbf{0}$	$\mathbf{0}$	$\mathbf{0}$	$\mathbf{0}$	0
$\vdots$	$\vdots$	$\ddots$	$\vdots$	$\vdots$	$\vdots$	$\vdots$	$\vdots$	$\vdots$	$\vdots$	$\vdots$	$\vdots$	$\vdots$	$\vdots$
$x_{i,r'}$	0	$\dots$	1	$\dots$	0	$\mathbf{1}$	$\mathbf{1}$	$\mathbf{1}$	$\mathbf{1}$	$\mathbf{1}$	$\mathbf{1}$	$\mathbf{1}$	1
$\vdots$	$\vdots$	$\vdots$	$\vdots$	$\ddots$	$\vdots$	$\vdots$	$\vdots$	$\vdots$	$\vdots$	$\vdots$	$\vdots$	$\vdots$	$\vdots$
$x_{i,\lvert\bar{R}_i\rvert}$	0	$\dots$	0	$\dots$	1	$\mathbf{0}$	$\mathbf{0}$	$\mathbf{0}$	$\mathbf{0}$	$\mathbf{0}$	$\mathbf{0}$	$\mathbf{0}$	0
$x_{i+1,R_{i+1}}$			$\mathbf{0}$			$\mathbf{0}$	$\mathbf{0}$	$\mathbf{0}$	$\mathbf{0}$	$\mathbf{I}$	$\mathbf{0}$	$\mathbf{0}$	0
$\vdots$			$\vdots$			$\vdots$	$\vdots$	$\vdots$	$\vdots$	$\ddots$	$\ddots$	$\vdots$	$\vdots$
$x_{\lvert\mathcal{I}\rvert,R_{\lvert\mathcal{I}\rvert}}$			$\mathbf{0}$			$\mathbf{0}$	$\mathbf{0}$	$\mathbf{0}$	$\mathbf{0}$	$\mathbf{0}$	$\mathbf{0}$	$\mathbf{I}$	0

Appendix B

Table 3: Computational results for the MIP formulations with flow- and cut-based contiguity under DATASET2 and SETUP1 in 3,600 seconds

		Best Incumbent		Best Bound		B&B (#)		Time in sec (gap in %)	
τ_{max}	Phase	w/o heur.	w/ heur.	w/o heur.	w/ heur.	w/o heur	w/ heur.	w/o heur.	w/ heur.
500 (flow)	1	0.67	NA	0.68	NA	356,142	NA	2,433	NA
	2	-	0.76	-	0.74	-	352,562	-	(2.86)
500 (cut)	1	0.67	NA	0.68	NA	910,800	NA	(1.91)	NA
	2	-	0.75	-	0.74	-	1,989,333	-	1,709
600 (flow)	1	0.67	0.68	0.69	0.69	174,542	163,444	(2.02)	(1.46)
	2	-	0.72	-	0.72	-	260,488	-	3,534
600 (cut)	1	0.68	0.67	0.69	0.69	336,213	2,883,598	(1.31)	(2.49)
	2	-	0.75	-	0.72	-	2,505,677	-	(3.31)
700 (flow)	1	0.68	0.68	0.69	0.69	96,894	112,982	(1.18)	(1.46)
	2	-	0.74	-	0.72	-	140,389	-	(2.73)
700 (cut)	1	0.67	0.68	0.69	0.69	136,720	2,144,472	(2.32)	(1.13)
	2	-	1.20	-	0.72	-	2,134,625	-	(39.56)

Appendix C

Table 4: Computational results of the MIP formulations with circular contiguity under DATASET2 and SETUP2 in 3,600 seconds

		Best Incumbent		Best Bound		B&B (#)		Time in sec (gap in %)	
τ_{max}	Phase	w/o fix	w/ fix	w/o fix	w/ fix	w/o fix	w/ fix	w/o fix	w/ fix
450	1	0.60	0.60	0.61	0.61	0	0	36	23
	2	0.64	0.64	0.63	0.63	143	667	85	97
500	1	0.61	0.61	0.61	0.61	0	375	47	54
	2	0.65	0.65	0.63	0.63	27,201	26,507	(4.21)	(3.56)
550	1	0.61	0.61	0.62	0.62	35	0	81	59
	2	0.63	0.65	0.62	0.62	720	18,901	472	(3.86)
600	1	0.62	0.62	0.62	0.62	684	3,625	443	617
	2	0.64	0.66	0.62	0.62	7,750	15,196	(2.96)	(5.60)
650	1	0.62	0.62	0.62	0.62	166	32	230	143
	2	0.65	0.68	0.62	0.62	7,366	14,150	(4.00)	(8.32)
700	1	0.62	0.62	0.62	0.62	227	31	254	174
	2	0.65	0.68	0.62	0.62	12,386	15,940	(3.76)	(8.32)